*remote sensing*

MDPI

*Article*

# Impact of Satellite Attitude on Altimetry Calibration with Microwave Transponders

**Costas Kokolakis [1,2,*], Dimitrios Piretzidis [2] and Stelios P. Mertikas [1]**

[1] Geodesy and Geomatics Engineering Laboratory, Technical University of Crete, GR-73100 Chania, Greece
[2] Space Geomatica P.C., Xanthoudidou 10A, GR-73134 Chania, Greece
* Correspondence: kkokolakis1@tuc.gr

**Abstract:** Satellite altimetry plays a key role in monitoring changes in sea level and climate change. The quality of satellite altimetry products is commonly ensured through dedicated calibration. One such calibration is with microwave transponders acting as ground reference point targets. It is common practice that satellite ranges between the transponder phase center and the satellite center of gravity (CoG) are compared against the true geometric ranges to determine bias. Transponder ranges are, however, realized by the two phase centers of the altimeter and the ground transponder. So, to make this comparison feasible, the space origin of the measured range is transferred from the altimeter phase center (APC) to the satellite CoG by applying a constant offset, usually referred to as "CoG correction". Instead of a fixed "CoG correction", this work introduces the actual vector between APC and CoG in space, by examining the satellite attitude. Thus, the observed and geometric distances to the transponder are both referred to the APC. The case of Jason-3 and Sentinel-6A Michael Freilich (Sentinel-6A MF) with two transponders on Crete (CDN1) and Gavdos (GVD1) islands is examined. At first, the attitude of Jason-3 is determined by its quaternions. Then, analysis reveals that the transponder bias is correlated with the Jason-3 satellite attitude. The revised calibration brings about bias changes which fluctuate from about −2 mm to 1 mm in range and from −110 μs to +110 μs in datation for Jason-3. Spectral analysis on the bias differences between the revised and conventional transponder calibrations reveals constituents with periods of 117, 39 and 23 days. Finally, the revised methodology on crossover calibrations over the GVD1 transponder results in an improvement between the mean bias of the ascending and descending orbits by 12% for Jason-3 and by 14% (preliminary) for Sentinel-6A MF.

**Keywords:** satellite altimetry; calibration; satellite attitude; Jason-3; Sentinel-6A MF



**Citation:** Kokolakis, C.; Piretzidis, D.; Mertikas, S.P. Impact of Satellite Attitude on Altimetry Calibration with Microwave Transponders. *Remote Sens.* **2022**, *14*, 6369. https://doi.org/10.3390/rs14246369

Academic Editor: Kaoru Ichikawa

Received: 29 November 2022
Accepted: 12 December 2022
Published: 16 December 2022



## 1. Introduction

One of the most important regulators of Earth's climate and thus key indicators in understanding climate is the ocean. Specifically, sea level is a fundamental environmental parameter as it reflects variations of multiple Earth mechanisms and physical processes [1]. Additionally, sea level rise is one of the most certain and threatening consequences of climate change [2]. A rise of 30 cm would push coastlines inwards by about 30–100 m [3] and thus cause destructive erosion, contamination of fresh water resources, reduction of agricultural soils and floods that endanger human lives. The importance of sea level for society led it to be included in the 50 essential climate variables (ECV) by the Global Climate Observing System [4] and the 13 ECVs monitored by the Climate Change Initiative [5] of the European Space Agency.

Sea level changes are primarily estimated and monitored on a global scale by satellite altimetry. About 20 satellite altimetry missions spanning more than 30 years provide products for various geophysical parameters that are crucial for the majority of Earth observing programs. These geophysical parameters are related to open ocean, near-coast areas, inland waters and ice-caps [6–9]. Moreover, some of the altimetric products that

are routinely used in geophysical analysis and climate studies are the sea surface height, wave height, wind speed, ionospheric total electron content, sea and land ice coverage and polar region topography [10–15]. These products are the starting point for scientific research, interpretation and important decision making that can largely impact society. Thus, systematically assessing the accuracy and validity of altimetric products should be treated as indispensable elements of all operational satellite altimetry missions.

The altimetric range, which is used for the direct calculation of sea surface heights, is continuously monitored for its quality to identify potential instrumental errors, drifts, etc. Altimetric ranges of one mission are also assessed with respect to other missions for identifying relative effects. Continuously monitoring the accuracy, homogeneity, and reliability of altimetric ranges is performed by external and independent facilities dedicated to Calibration/Validation (Cal/Val). The Cal/Val techniques developed for this purpose are generally classified into two main categories: those which rely on reference infrastructures deployed at sea (e.g., buoys) or on coasts (e.g., tide gauges) and those that rely on point targets operating on land (e.g., active transponders and corner reflectors). The present analysis is focused on the latter category (i.e., calibration of altimetric ranges using a transponder) and utilizes measurements acquired by two Ku-band microwave transponders of the Permanent Facility for Altimeter Calibration (PFAC) of ESA, installed on Crete (CDN1 site) and Gavdos (GVD1 site) islands.

Although altimeter calibration using a transponder has been proposed in the past [16], its practical implementation has not evolved accordingly to align with algorithmic and technological developments. The altimetry community has now acknowledged that satellite attitude needs to be taken into account in altimetry data processing. The Ocean Surface Topography Science Team (OSTST) Meeting in 2019 [17], recommends to include attitude information in Geophysical Data Record (GDR) products, and for the older altimeters.

Up to now, effects arising from satellite attitude have been routinely considered in precise orbit determination (POD). Satellite attitude is realized in POD by either a priori attitude models (called "nominal" attitude), or by on-board measurements realized by star tracker cameras. Recent results [18] show that the use of observation-based attitude improves orbit determination with Satellite Laser Ranging (SLR) for the Jason series. An improvement of about 4.5–8.3% in the orbit RMS is reported in [18] when using the observation-based attitude instead of the nominal model. In addition, when POD results for Jason-3 are determined using the observation-based attitude, it leads to an average RMS of 3.29 cm instead of 4.13 cm with the nominal attitude model [19].

Besides orbit determination, non-ideal attitude has an additional effect on altimetric measurements and ocean products. In [20,21], a correction was proposed for the measured ocean range of Geosat and TOPEX/Poseidon altimeters, respectively. This correction accounted for instrument biases due to significant wave height and attitude (off-nadir) angle, estimated from the averaged return waveform using the Brown model. A degradation of the Jason-1 star tracker system was observed in April 2002, which led to abnormally large attitude angles and a reduced accuracy of altimetric products derived by conventional retracking algorithms. To account for these large attitude angles, a second-order analytical model for the altimeter echo and a four-parameter maximum likelihood estimator was proposed in [22]. Their method resulted in a reduction in the bias of the geophysical parameters estimated by the averaged return waveforms. In [23], the attitude angle was identified as a potential indicator for detecting anomalies in the significant wave heights estimated from SARAL/AltiKa altimetric waveforms. Non-ideal attitude is also known to cause distortions on the measurements of altimeters operating in synthetic aperture radar (SAR) mode. More specifically, a pitch angle can result in asymmetries in the echo power distribution of forward- and backward-looking beams. This effect has been studied by [24] to independently estimate the pitch angle of CryoSat-2. Finally, attitude-dependent corrections have been implemented in [25] to account for non-uniform heating of the microwave radiometer and improve the estimation of wet troposphere delays.

A systematic review of the literature on satellite altimeter calibration using a transponder indicates that attitude effects have neither been examined nor taken into account in this context [26–31]. The non-ideal satellite attitude has been recognized in [32] as a potential source of uncertainty affecting the altimeter antenna gain, which should always be evaluated in the altimeter-to-transponder line-of-sight direction. Following the advancements and recommendations in recent altimetry studies, the standard procedure of calibration using a transponder should be revised accordingly to account for satellite attitude effects. In this work, we propose and test a methodology for incorporating attitude information into the calibration procedure. Our main objective is to improve the estimation of range and datation biases by mitigating systematic errors coming from the nominal offset between the altimeter phase center (APC) and the satellite center of gravity (CoG). We therefore design an analytical method for the rigorous calculation of the offset between the APC and CoG based on the instantaneous orientation of the satellite in three-dimensional space. We then use this offset to refer all measurements used in the calibration to APC. Since our method is completely based on readily available data, it can be easily implemented by calibration teams without the need for any special pre-processing performed prior to the distribution of altimetric products from the processing Agencies. The proposed calibration methodology is comprehensive and can be applied to every past, current and future altimetry mission with available attitude measurements.

We use our approach to evaluate and study attitude effects on range and datation biases for the calibration of Jason-3. The selection of Jason-3 is motivated by the long time series of transponder calibrations made at the CDN1 Cal/Val, spanning from 2016 to 2022. Jason-3 was also selected because it has been the reference altimetry mission since 2016, up until Sentinel-6A Michael Freilich (Sentinel-6A MF) succeeded in this role in 2022. Furthermore, its ∼10-day repeat track orbit is more frequent compared to other satellites, such as Haiyang-2 (∼14 days) or Sentinel-3 (∼27 days). Based on this fact, Jason-3 offers a time series of range and datation biases with finer temporal resolution, which increases the reliability of spectral analysis. Finally, the necessary datasets for calibration processing (SGDR version F, attitude information, etc.) are publicly available and cover its entire lifespan.

This paper is structured as follows. Section 2 describes the ESA PFAC infrastructure, its instrumentation, Cal/Val site distribution and current Cal/Val activities. Section 3 discusses the determination of attitude angles, the fundamental methodology for the calculation of range and datation biases using a transponder and the application of the revised processing accounting for attitude effects. The most important findings are presented and discussed in Section 4. Finally, Section 5 provides the main conclusions of this investigation.

## 2. Ground Cal/Val Infrastructure

The ground infrastructure of the PFAC is located in west Crete, Greece (Figure 1). It is dedicated to satellite altimetry Cal/Val activities by providing both indirect (sea-surface) and direct (transponder) absolute calibrations of all overflying altimeters. Established in 2004, the PFAC has been delivering bias results for every international altimetry mission, such as Jason-1/2/3, SARAL/AltiKa, HaiYang-2A & B, CryoSat-2, Sentinel-3A & B and Sentinel-6A MF [33]. It consists of (a) four permanent sea-surface calibration sites, namely the GVD8 Cal/Val site on Gavdos island, the CRS1, SUG1 and RDK1 Cal/Val sites in southwest Crete, and (b) two Ku-band (central frequency 13.575 GHz) transponder sites for absolute calibration of satellite altimeters [29].

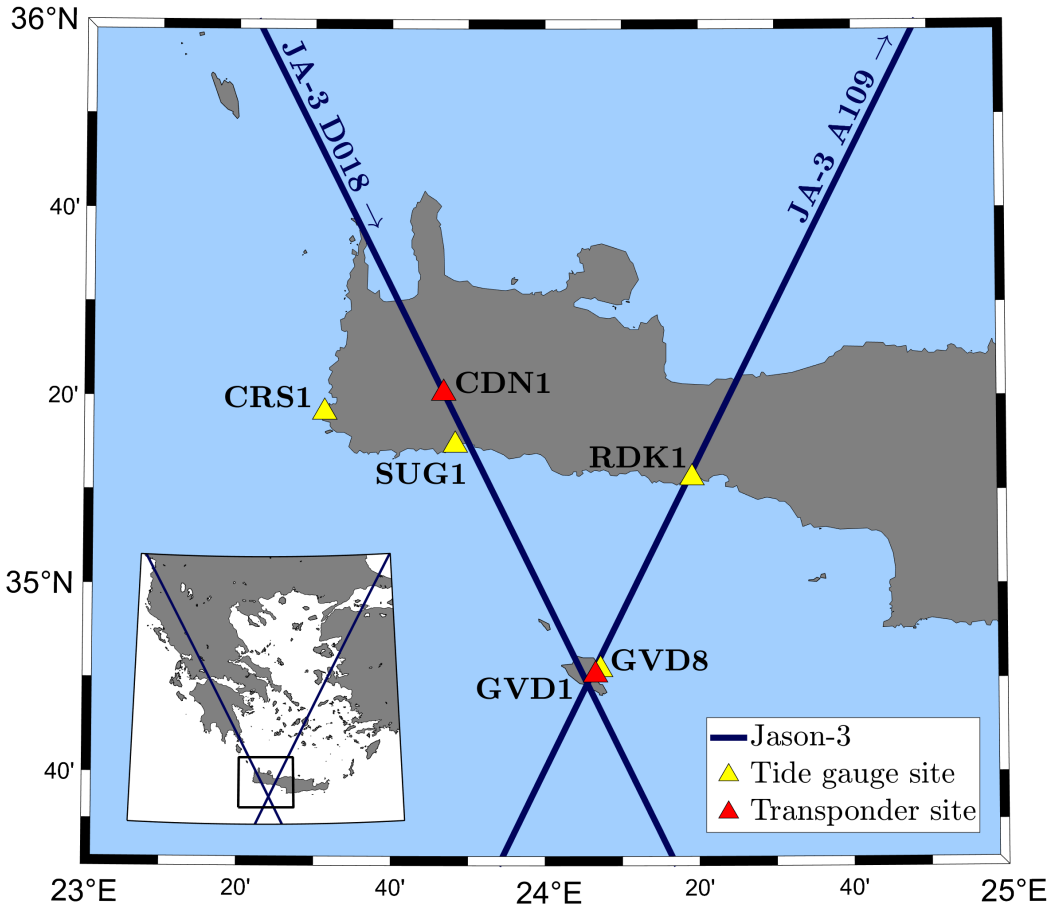


**Figure 1.** A map of the PFAC infrastructure with Jason-3 orbits forming a crossover at Gavdos island.

The first transponder site, named CDN1, is located in a mountainous region at an elevation of about 1050 m in the western part of Crete and has been continuously operational since September 2015. The second site, named GVD1, was established at an elevation of 98 m on Gavdos island in October 2021 and has also been continuously operational since then.

With regard to the reference orbits of Jason-3 and Sentinel-6A MF, the CDN1 transponder site has been used for the calibration of their descending pass D018. The GVD1 transponder site, located on a crossover point, provides calibrations for D018 about 11 s after the CDN1 calibration of the same pass and calibrations for the ascending pass A109 about 5 days after the calibration of D018. Apart from the principal instrument of a transponder, each Cal/Val site is equipped with additional instrumentation required for calibration, such as permanent Global Navigation Satellite System (GNSS) stations, meteorological sensors, microwave radiometer, etc. A detailed description of the infrastructure and all geophysical corrections necessary for calibrations can be found in [29].

Both transponder Cal/Val sites are compliant with the strategy of Fiducial Reference Measurements (FRM), established by ESA for satellite calibrations [34,35]. This FRM strategy entails, among other things, reporting of every constituent of uncertainty associated to the calibration process before calculating the final uncertainty of the altimeter bias. Moreover, FRM asks for redundancy of scientific instrumentation (different manufacturers, diverse measuring principles, various setups, etc.) and diversity in the techniques and methods to estimate the bias. Following these guidelines, every key parameter for altimetry calibration is estimated using different approaches and methodologies. For example, transponder coordinates are determined by relative GNSS positioning and precise point positioning, while tropospheric delays are estimated using GNSS observations, radiometers and satellite sensors (e.g., Ocean and Land Color Instrument on board Sentinel-3A & B) [36].

## 3. Satellite Attitude and Transponder Calibration

### *3.1. Determination of the Satellite Attitude*

In this Section, the Jason-3 satellite will be used as an example to demonstrate the applied methodology of attitude determination and its impact on transponder calibration. The Jason-3 spacecraft was designed based on a "box-wing" structural model and consists of the spacecraft bus (box) and the solar panel arrays (wings). The main scientific payload of Jason-3 comprises the Poseidon-3B (P3B) dual frequency (13.575 GHz and 5.3 GHz) nadir-looking radar altimeter, a microwave radiometer, a precise orbit determination system (PODS) and an attitude determination and control system (ADCS) [37].

The PODS is responsible for the determination of the satellite's position in space and consists of a Doppler Orbitography and Radiopositioning Integrated by Satellite (DORIS) receiver, a GNSS receiver and a laser retroreflector array. The ADCS provides the satellite's three-dimensional orientation via the combined analysis of measurements coming from star trackers, magnetometers, sun sensors, magnetic torquers and gyroscopes. The star trackers have optical sensors that capture snapshots of the sky to calculate the positions of specific stars. Comparison of the observed position of stars with the corresponding one from the on-board ephemeris results in the accurate estimation of spacecraft attitude.

The instantaneous orientation of the satellite is used by an attitude actuation mechanism, consisting of reaction wheels, to perform attitude adjustments. The two attitude criteria for a reliable operation of the satellite are as follows. Firstly, the altimeter boresight should point downwards and perpendicularly to the reference ellipsoid (nadir-pointing). This criterion is necessary for the altimeter to receive reliable return waveforms, following their reflection on the ocean surface. Secondly, the solar panels direction should be perpendicular to the Sun arrays in order to provide and store adequate power to the satellite. The above requirements were firstly realized in the TOPEX/Poseidon altimeter using the algorithms described in [38]. The same algorithm principles are also used for the adjustment of Jason-3 attitude.

The following reference systems need to be defined for the estimation of satellite attitude and the post-processing of altimetric products [39]:

- The inertial reference system (IRS; [O: $UVW$]), with its origin at the geocenter O. It is a system that does not rotate with the Earth, and its axes are parallel to the barycentric system whose origin is at the Sun. The $U$ axis passes from the equatorial plane with direction towards the vernal equinox $\Upsilon$. The $W$ axis coincides with the Earth's mean rotation axis, and the $V$ axis is perpendicular to the $U$ axis to form a right-hand orthogonal reference system. This system is also referred to as "pseudo-inertial" because of the acceleration arising from the Earth's revolution around the Sun.
- The Earth-fixed reference system (EFRS; [O: $XYZ$]), with its origin at the geocenter O. It is a reference system that rotates with the Earth's angular velocity. Its origin O also coincides with the center of the reference ellipsoid, i.e., the WGS84 ellipsoid for the latest processing baseline (F) of Jason-3 products. The $X$ and $Y$ axes are located at the equatorial plane with directions towards the prime meridian ($\lambda = 0°$) and perpendicular to it ($\lambda = 90°$), respectively. The $Z$ axis coincides with the Earth's rotation axis with direction towards the North Pole.
- The satellite body reference system (SAT; [Q: $x_B y_B z_B$]), with its origin at the center $Q$ of the launcher attachment ring on the satellite. The $x_B$ axis is parallel to the satellite primary direction and towards the radiometer antenna. The $y_B$ axis is parallel to the rotation axis of the solar panels with direction towards the right solar panel array. The $z_B$ axis direction is chosen to form an orthogonal right-handed reference system. Ideal attitude of the satellite body is realized when the $z_B$ axis is perpendicular to the reference ellipsoid.
- The orbital reference system (ORB; [K: $xyz$]), with its origin at the satellite CoG (denoted by K in Figure 2). The $x$ axis is along the radial vector connecting the geocenter $O$ and the satellite CoG, K, with direction towards the zenith (reverse geocentric positioning [40]). The $z$ axis is perpendicular to the satellite orbital plane

with the same direction as the orbital angular momentum. Finally, the $y$ axis has a direction to complete a right-hand orthogonal reference system (i.e., towards the satellite velocity vector but not always parallel to it).

- The local orbital reference system or roll-pitch-yaw system (RPY; [K: $x_0y_0z_0$]), has its origin at the satellite CoG, K. Its $z_0$ axis (yaw) is perpendicular to the reference ellipsoid with a direction towards nadir. The $y_0$ axis (pitch) is perpendicular to the orbital plane with direction opposite to angular momentum. Finally, the $x_0$ axis (roll) is defined to form an orthogonal reference system, with the same direction as the satellite velocity vector.

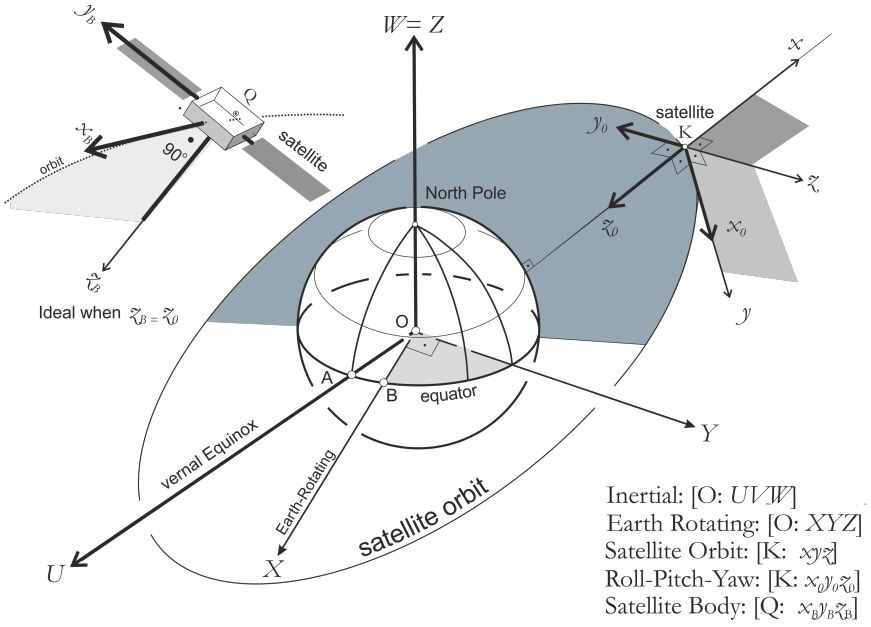


**Figure 2.** Graphical representation of fundamental reference systems used for satellite attitude determination. The direction OA is defined by the vernal equinox ♈, and the direction OB denotes the prime meridian ($\lambda = 0°$).

The reference systems listed above are presented in Figure 2. The satellite attitude corresponds to the three-dimensional orientation of the satellite spacecraft in space, and it is commonly described by the roll, pitch and yaw angles, i.e., the angles needed to be applied in order to transform a vector from RPY to SAT system. In the sequel, the fundamental expressions used to estimate the satellite attitude angles are provided.

The transformation of a column-vector $\mathbf{X}_\mathrm{I} = [U, V, W]^\mathrm{T}$ to $\mathbf{X}_\mathrm{S} = [x_B, y_B, z_B]^\mathrm{T}$, i.e., from the inertial IRS to the satellite body reference system SAT is performed as:

$$\mathbf{X}_\mathrm{S} = \begin{bmatrix} x_B \\ y_B \\ z_B \end{bmatrix} = \mathbf{R}_{\mathrm{IRS}\to\mathrm{SAT}} \begin{bmatrix} U \\ V \\ W \end{bmatrix} = \mathbf{R}_{\mathrm{IRS}\to\mathrm{SAT}}\mathbf{X}_\mathrm{I}, \tag{1}$$

where the matrix $\mathbf{R}_{\mathrm{S1}\to\mathrm{S2}}$ denotes the rotation matrix (square matrix) that transforms a vector from reference system S1 to S2. The rotation matrix $\mathbf{R}_{\mathrm{IRS}\to\mathrm{SAT}}$ is calculated using information stored in quaternions and can be expressed by the following sequence of rotations [18]:

$$\mathbf{R}_{\mathrm{IRS}\to\mathrm{SAT}} = \mathbf{R}_{\mathrm{RPY}\to\mathrm{SAT}}\mathbf{R}_{\mathrm{ORB}\to\mathrm{RPY}}\mathbf{R}_{\mathrm{IRS}\to\mathrm{ORB}}. \tag{2}$$

Solving Equation (2) with respect to $\mathbf{R}_{\mathrm{RPY}\to\mathrm{SAT}}$ yields

$$\mathbf{R}_{\mathrm{RPY}\to\mathrm{SAT}} = \mathbf{R}_{\mathrm{IRS}\to\mathrm{SAT}}\mathbf{R}^\mathrm{T}_{\mathrm{IRS}\to\mathrm{ORB}}\mathbf{R}^\mathrm{T}_{\mathrm{ORB}\to\mathrm{RPY}}, \tag{3}$$

where the relation $\mathbf{R}_{S1\to S2}^{T} = \mathbf{R}_{S1\to S2}^{-1} = \mathbf{R}_{S2\to S1}$ applies, as a rotation matrix is always orthogonal and thus its transpose will be equal to its inverse. The rotation matrix $\mathbf{R}_{IRS\to ORB}$ can be derived from the satellite state vector (i.e., position vector $\mathbf{r}$ and velocity vector $\mathbf{v}$) in the IRF system, as follows:

$$\mathbf{R}_{IRS\to ORB} = \begin{bmatrix} \mathbf{R}_1 & \mathbf{R}_2 & \mathbf{R}_3 \end{bmatrix}^{T}, \tag{4}$$

with the components $\mathbf{R}_1$, $\mathbf{R}_2$ and $\mathbf{R}_3$ defined as

$$\mathbf{R}_1 = \frac{\mathbf{r}}{|\mathbf{r}|}, \quad \mathbf{R}_3 = \frac{\mathbf{r}\times\mathbf{v}}{|\mathbf{r}\times\mathbf{v}|}, \quad \mathbf{R}_2 = \mathbf{R}_3 \times \mathbf{R}_1, \tag{5}$$

and the rotation matrix $\mathbf{R}_{ORB\to RPY}$ given by

$$\mathbf{R}_{ORB\to RPY} = \begin{bmatrix} 0 & 1 & 0 \\ 0 & 0 & -1 \\ -1 & 0 & 0 \end{bmatrix}. \tag{6}$$

After the calculation of $\mathbf{R}_{RPY\to SAT}$ from Equation (2) through (6), the evaluation of roll, pitch and yaw angles, denoted as $\theta_r$, $\theta_p$ and $\theta_y$, respectively, is performed using the elements of $\mathbf{R}_{RPY\to SAT}$, as follows:

$$\theta_r = -\arctan\left(\frac{\mathbf{R}(3,2)}{\mathbf{R}(3,3)}\right), \quad \theta_p = \arcsin\left(\mathbf{R}(3,1)\right), \quad \theta_y = -\arctan\left(\frac{\mathbf{R}(2,1)}{\mathbf{R}(1,1)}\right), \tag{7}$$

with $\mathbf{R}(i,j)$ denoting the $i$-th row and $j$-th column element of the rotation matrix $\mathbf{R}$. All rotation angles are considered passive (i.e., the reference systems are actually rotated and not the contextual vectors) and positive in the counter-clockwise direction.

### *3.2. Range and Datation Bias*

The range bias of a satellite altimeter represents the systematic error in measuring distances. This bias is estimated by comparing the altimeter (or measured) range with the corresponding geometric distance (considered the "true" value) between the satellite CoG and the reflecting target (in this work the microwave transponder). The initial estimation of the measured range is typically performed by the altimeter tracker or by a retracking algorithm and is based on the return waveform. The shape of the return waveform is described by the Brown model [41] over ocean regions and by a point target response (PTR) over transponders. A profile map of the PFAC transponder sites and the Jason-3 return waveforms transitioning between a Brown model and a PTR is presented in Figure 3.

In the context of calibration with a transponder, a number of corrections need to be applied to the measured and geometric ranges to correctly estimate the altimeter range bias [29]. The corrections to the initial measured range (i.e., tracker range) are applied partially from the processing Agencies and the Cal/Val teams. Conventional corrections applied by the processing Agencies account for the offset distance between the APC and satellite CoG, the ultra-stable oscillator (USO) drift, internal path delay and instrumental and system errors. The corrections applied by the Cal/Val teams are due to the effects of the ionosphere and troposphere (atmospheric delays), the transponder internal path delay and the Doppler effect as a consequence of the relative velocity of the altimeter satellite with respect to the transponder. Additional corrections are applied to the geometric range to account for displacements of the transponder position caused by tidal and non-tidal effects of atmosphere, solid Earth, pole and ocean loading.

The offset between APC and CoG, also known as "CoG correction", is associated with satellite attitude. Given the objectives of this study, we isolate this parameter from the rest of the corrections and examine how its current implementation influences bias results. Based on the information given in the beginning of this section, the range bias $B(t)$ is defined as follows:

$$B(t) = r(t) - r_0(t), \tag{8}$$

where $r(t)$ and $r_0(t)$ denote the corrected measured range and corrected geometric range, respectively, both of which refer to the satellite CoG. Since both ranges change as the satellite flies over the transponder, they are functions of time $t$. The range $r(t)$ is written in terms of the corrected measured range $R(t)$ referred to the APC, as follows:

$$r(t) = R(t) + \delta r, \tag{9}$$

with $\delta r$ being the CoG correction. The corrected geometric range $r_0(t)$ is calculated by:

$$r_0(t) = \sqrt{\left(X^{\mathrm{TRP}} - X^{\mathrm{CoG}}(t)\right)^2 + \left(Y^{\mathrm{TRP}} - Y^{\mathrm{CoG}}(t)\right)^2 + \left(Z^{\mathrm{TRP}} - Z^{\mathrm{CoG}}(t)\right)^2}, \tag{10}$$

where $(X, Y, Z)$ are the coordinates of the transponder (superscript TRP) and satellite CoG (superscript CoG) in the Earth-fixed reference system. In Equation (10), it is assumed that the transponder coordinates are constant for a specific cycle.

A second type of bias estimated during the calibration of an altimetric system is the datation (or time-tagging) bias. This bias provides information regarding the error made on the reference time of the altimetric measurements [42]. The definition of datation bias is based on the time of closest approach (TCA), which represents the time at which the distance between transponder and satellite is minimized. Two types of TCA are associated with the calculation of datation bias. The first one is the time at which the corrected measured range is minimized, and the second one is the time at which the corrected geometric range is minimized. Since the histories of both ranges form a parabolic curve over a transponder (Figure 3), the two TCAs denote the vertex position of the corresponding parabolas. The datation bias is defined as the difference between the two TCAs, as follows

$$dt = \underset{t \in \mathbb{R}_+}{\arg\min}\, r(t) - \underset{t \in \mathbb{R}_+}{\arg\min}\, r_0(t), \tag{11}$$

where the function $\arg\min_x f(x)$ returns the value of $x$ that minimizes $f(x)$.

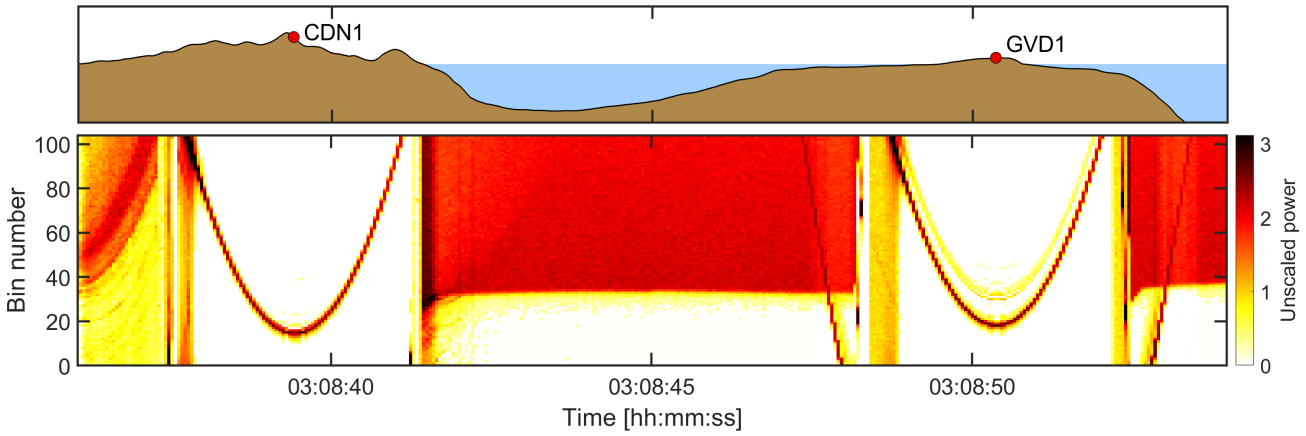


**Figure 3.** Topographic and bathymetric profile along the Jason-3 D018 (descending) pass, starting from the north with the CDN1 transponder in Crete, passing over the sea region between Crete and Gavdos, and reaching the GVD1 transponder south in Gavdos. The generated averaged waveforms of the transponder signals are also shown (bottom).

### *3.3. Calibration Accounting for Satellite Attitude*

For altimeter calibration with a transponder, it is common practice that the corrected measured range $r(t)$ is used for the evaluation of range and datation biases based on Equations (8) and (11), respectively. As already described in Section 3.1, this measured range is transferred from APC to CoG by the processing Agencies using the CoG correction $\delta r$. The description provided in the product handbook of each altimetry mission states that

the CoG correction is defined as the distance along the z-axis between APC and CoG in the satellite body reference frame. Since this parameter is derived using the geometry of the spacecraft, its value is constant for the entire duration of a mission and for its observations. A review of previous investigations showed that the measured range used for calibration is indeed referred to CoG. For example, Hausleitner et al. [27] mentions that the Jason-2 altimeter range is referred to the CoG, by applying a CoG correction, given in the GDR products. Inspection of Jason-2 GDR products reveals that this parameter is in fact constant. The work of Cristea and Moore [26] also mentions that a constant CoG offset is also applied to reduce the observed range for the satellite geometry prior to the calculation of EnviSat range bias using a transponder.

It is important to examine the implications of applying a constant CoG correction to the measured range instead of a varying correction originated from alterations in satellite attitude. We firstly discuss the case of altimetric measurements over oceans. Figure 4a shows an example of an ideal attitude for an orbiting satellite, where its altimeter antenna points perpendicularly to the ellipsoid. The ocean surface point, OCN1, can be considered a nadir-located target. The line segments |OCN1, APC|, |APC, CoG′| and |OCN1, CoG′| represent the observed range referred to APC, the constant CoG correction and the observed range referred to the CoG′, respectively. The CoG′ point represents the apparent CoG of the satellite at which the measured range $r(t)$ is referred to after applying the CoG correction $\delta r$ using Equation (9). Finally, the line segment |OCN2, CoG| denotes the distance between the true CoG and the sea surface. From the geometry of Figure 4a, it is evident that, for an ideal attitude, the distances |OCN1, CoG′| and |OCN2, CoG| are equal. It is therefore reasonable to consider that the measured range is correctly referred to the true CoG when the constant distance between APC–CoG along the z-axis is used.

Figure 4b shows the case of non-ideal attitude, where only a pitch rotation (exaggerated) is displayed for simplicity. Assuming that all rotations are performed with respect to the CoG, the non-ideal attitude results in a change in the position of APC and thus CoG′. As a consequence, |OCN1,CoG′| distance is no longer equal to |OCN2,CoG| distance, and therefore the measured range is not realistically referred to the true CoG.

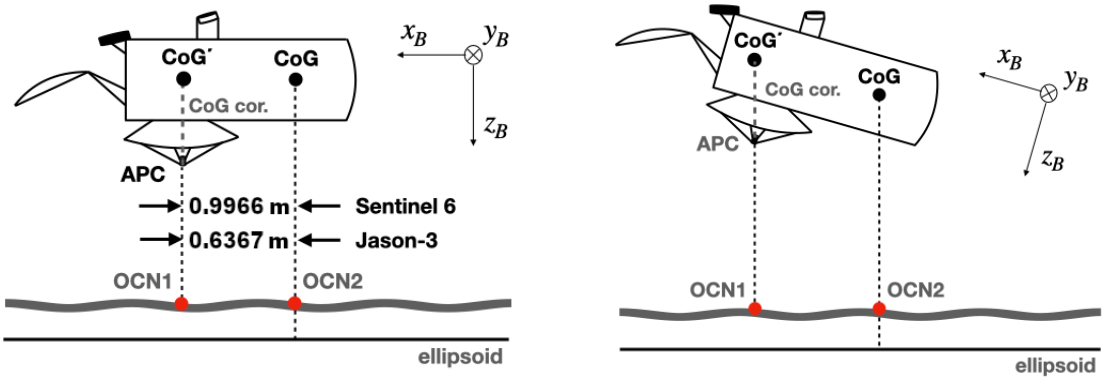


**Figure 4.** Altimetric measurement acquisition over sea surface for (**a**) ideal and (**b**) non-ideal satellite orientation. The axes of the SAT system (satellite body system) are also presented.

We continue by examining the impact of satellite attitude on altimetric measurements acquired over point targets (e.g., during an altimeter calibration with a transponder). A fundamental difference here is that, unlike ocean surface, transponders are practically never located directly at the nadir of the altimeter antenna. This is because the selection of a transponder site is limited by (a) the terrain topography and site accessibility based on existing road infrastructure, (b) the need to support the simultaneous calibration of multiple missions, and (c) the quality of the signal clutter in the area. Even if a transponder is installed at the nadir of a satellite based on its nominal orbit, the repeat ground track

location of a specific satellite pass can vary several hundreds of meters on the ground even for consecutive cycles.

The case of a satellite with ideal attitude passing over a transponder is given in Figure 5a. The CoG correction denoted by the equidistant line segments |APC;$B_0$| and |APC;B| is again applied to the measured range |APC;A| and accounts for the coordinate difference between APC and CoG in the $z_B$ direction. As a result, the measured range is referred to the apparent CoG, which corresponds to point B. The same also applies for non-ideal satellite attitude, as demonstrated in Figure 5b. It is evident in both cases that the corrected measured range |A;B| is not equal to the line segment |A;GoC|; therefore, the measured range $r(t)$ is not accurately referred to the satellite CoG.

From the discussion provided so far, it can be concluded that the conventional implementation of CoG correction is proper only when both of the following requirements are met: (a) ideal satellite attitude (i.e., zero attitude angles) and (b) targets located along the altimeter nadir. For satellites passing over transponders, none of these requirements are met. It is therefore reasonable to argue that during satellite calibration, the measured range $r(t)$ is not correctly referred to the CoG. On the contrary, the geometric distance $r_0(t)$ is rigorously referred to CoG, since the estimated CoG coordinates provided in the GDR products already account for attitude effects. This inconsistency has a direct impact on the evaluation of range bias using Equation (8). In addition, the different reference of the measured and geometric range can affect the TCA and introduce errors in the estimation of datation bias using Equation (11). The datation errors due to non-ideal attitude mostly depend on the relative position between B and CoG.

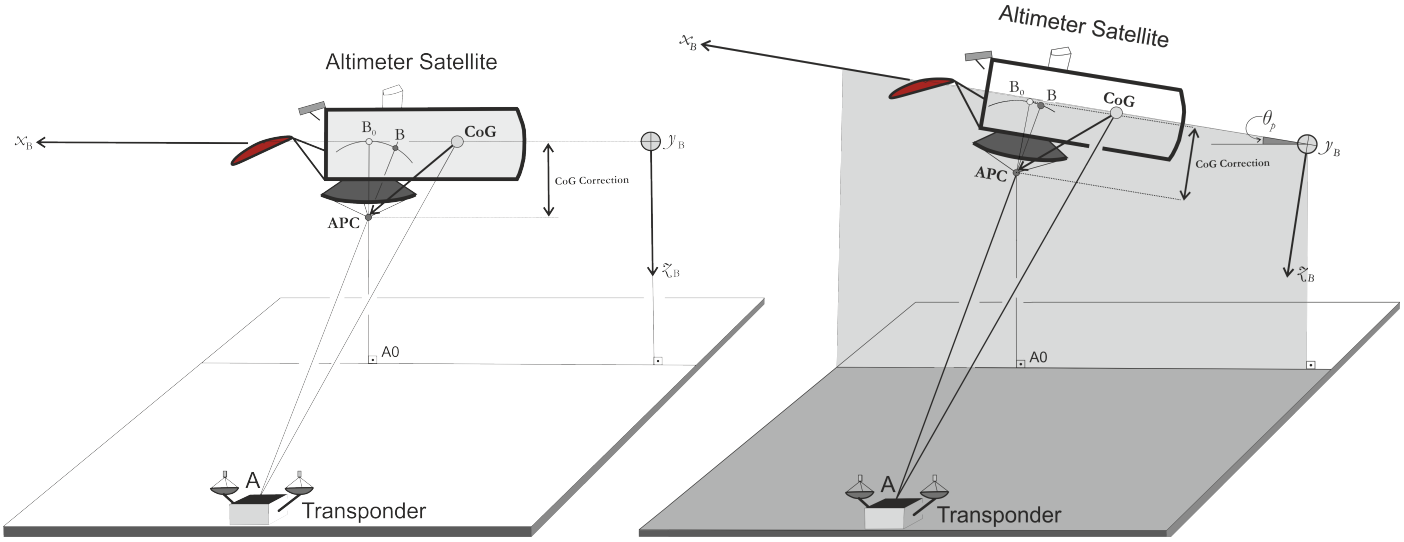


(**a**) (**b**)

**Figure 5.** Altimetric measurement acquisition over a transponder for (**a**) ideal and (**b**) non-ideal satellite orientation (when pitch is introduced). The vector with origin at the satellite's CoG and end at the APC is presented. The "CoG correction" is the distance added to the measured range (i.e., A, APC) to account for the APC offset. The axes of the satellite body reference system are also presented.

It is evident that attitude effects have an influence on transponder results and need to be further examined. An improved calibration procedure that accounts for these effects using attitude information is also required. A revisited calibration procedure is discussed in the rest of this section.

Attitude effects on transponder results can be corrected by rigorously referring the measured and geometric ranges to the same reference point using information regarding the instantaneous orientation of the spacecraft. In this work, we have chosen the APC as the reference point for all parameters related to the calculation of range and datation biases. The new range bias, denoted as $\widetilde{B}(t)$, is defined as:

$$\widetilde{B}(t) = R(t) - R_0(t), \tag{12}$$

where $R(t)$ and $R_0(t)$ are the corrected measured and corrected geometric ranges between transponder and APC. The calculation of $R(t)$ is performed using Equation (9) and only requires the subtraction of the constant CoG correction from the corrected altimeter range used in the conventional calibration procedure. The rest of the corrections (i.e., atmospheric delays, loading effects, etc.) are applied as usual. Following Equation (10), the geometric range $R_0(t)$ is defined as:

$$R_0(t) = \sqrt{\left(X^{\mathrm{TRP}} - X^{\mathrm{APC}}(t)\right)^2 + \left(Y^{\mathrm{TRP}} - Y^{\mathrm{APC}}(t)\right)^2 + \left(Z^{\mathrm{TRP}} - Z^{\mathrm{APC}}(t)\right)^2}. \tag{13}$$

It is evident from Equation (13) that the evaluation of the geometric range $R_0(t)$ requires the calculation of APC coordinates in EFRS. The APC coordinate vector in EFRS, denoted as $\mathbf{V}_{\mathrm{EFRS}}^{\mathrm{APC}} = [X^{\mathrm{APC}}, Y^{\mathrm{APC}}, Z^{\mathrm{APC}}]^{\mathrm{T}}$, can be determined using the relation:

$$\mathbf{V}_{\mathrm{EFRS}}^{\mathrm{APC}} = \mathbf{V}_{\mathrm{EFRS}}^{\mathrm{CoG}} + \Delta\mathbf{V}_{\mathrm{EFRS}}, \tag{14}$$

where $\mathbf{V}_{\mathrm{EFRS}}^{\mathrm{CoG}}$ is the CoG coordinate vector and $\Delta\mathbf{V}_{\mathrm{EFRS}}$ the CoG–APC baseline vector in EFRS. The vector $\mathbf{V}_{\mathrm{EFRS}}^{\mathrm{CoG}}$ corresponds to the satellite position as defined by orbit determination. The baseline vector $\Delta\mathbf{V}_{\mathrm{EFRS}}$ depends on the satellite attitude and is transformed from SAT system [Q: $x_B y_B z_B$] to EFRS system [O: $XYZ$] using the equation:

$$\Delta\mathbf{V}_{\mathrm{EFRS}} = \mathbf{R}_{\mathrm{SAT}\to\mathrm{EFRS}}\Delta\mathbf{V}_{\mathrm{SAT}} = \mathbf{R}_{\mathrm{IRS}\to\mathrm{EFRS}}\mathbf{R}_{\mathrm{SAT}\to\mathrm{IRS}}\Delta\mathbf{V}_{\mathrm{SAT}}. \tag{15}$$

The calculation of rotation matrix $\mathbf{R}_{\mathrm{IRS}\to\mathrm{EFRS}}$ for the transformation between IRS and EFRS is described in the IERS conventions 2010 [43,44]. The calculation of $\mathbf{R}_{\mathrm{SAT}\to\mathrm{IRS}}$ can be performed as already discussed in Section 3.2, and the evaluation of vector $\Delta\mathbf{V}_{\mathrm{SAT}}$ is based on the spacecraft geometry and mass properties that are provided in the corresponding mission documentation. The APC and CoG coordinates in the SAT system for Jason-3 and Sentinel-6A MF are given in Table 1. During the spacecraft operation, the CoG is subject to a minor displacement over time due to events such as fuel consumption (Figure 6). The precise evaluation of $\Delta\mathbf{V}_{\mathrm{SAT}}(t)$ at a specific time epoch $t$ is performed as follows:

$$\Delta\mathbf{V}_{\mathrm{SAT}}(t) = \Delta\mathbf{V}_{\mathrm{SAT}}(t_0) + \delta\mathbf{V}_{\mathrm{SAT}}(t). \tag{16}$$

The first term on the right-hand side of Equation (16) denotes the APC– CoG baseline vector as measured prior to the satellite deployment, and the second term denotes its temporal variations due to the CoG displacement [37]. The Jason-3 $x_B$-axis component of the CoG displacement in the SAT system is given in Figure 6, along with the spacecraft mass change.

**Table 1.** Coordinates of reference points (CoG and APC) in the SAT system for Jason-3 and Sentinel-6A MF [37,45].

| | Reference Points | $x_B$ (m) | $y_B$ (m) | $z_B$ (m) |
|---|---|---|---|---|
| Jason-3 | Spacecraft center of gravity | 1.0023 | 0.0000 | −0.0021 |
| | Altimeter phase center | 1.6390 | 0.0000 | 0.6644 |
| Sentinel-6A MF | Spacecraft center of gravity | 1.5274 | −0.0073 | 0.0373 |
| | Altimeter phase center | 2.5240 | 0.0001 | 0.5650 |

In line with Equation (11), the new datation bias, $\widetilde{dt}$, after referring all parameters to APC is given by:

$$\widetilde{dt} = \underset{t\in\mathbb{R}_+}{\arg\min}\, R(t) - \underset{t\in\mathbb{R}_+}{\arg\min}\, R_0(t). \tag{17}$$

We finally define the attitude effect on range and datation bias per cycle (denoted $\delta B$ and $\delta T$, respectively) as the bias difference before and after accounting for non-ideal attitude, i.e.,:

$$\delta B = \widetilde{B} - B, \tag{18}$$

and

$$\delta T = \widetilde{dt} - dt. \tag{19}$$

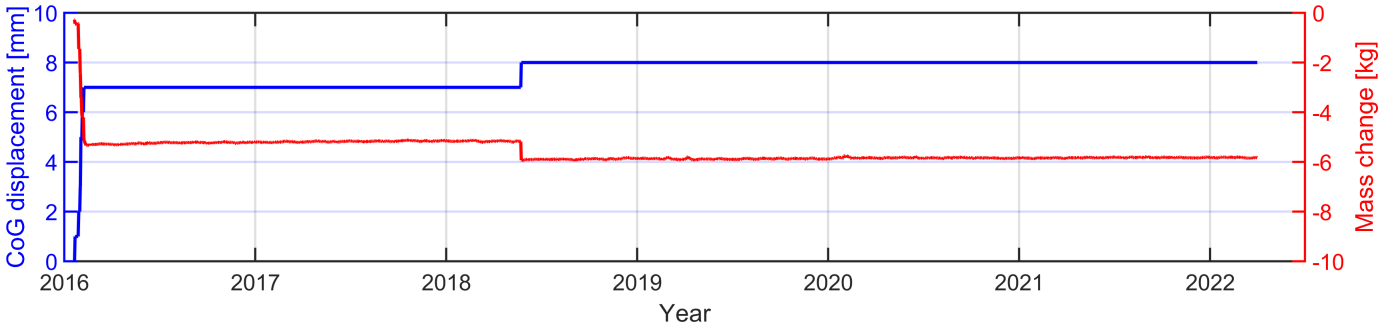


**Figure 6.** Jason-3 mass and CoG (x-component) history since deployment.

## 4. Results

### *4.1. Jason-3 Attitude Determination*

The Jason-3 attitude angles are evaluated at the TCA over CDN1 and GVD1 transponder sites for each cycle using the methodology of Section 3.1. The files containing the Jason-3 quaternion data for the construction of matrix $\mathbf{R}_{\mathrm{IRS}\to\mathrm{SAT}}$ are acquired from NASA's Crustal Dynamics Data Information System (CDDIS). Each quaternion file covers a time period of 28 h with a temporal resolution of 30 s. The data stored in consecutive quaternion files have a two-hour overlap. The quaternions at a specific TCA are estimated using spherical linear interpolation. Daily values of mass and CoG displacements for Jason-3 are obtained from the International DORIS Service (IDS). The estimation of CoG displacements at TCA is performed using linear interpolation. The estimated CoG displacements are then used for the calculation of $\delta\mathbf{V}_{\mathrm{SAT}}$ parameter.

The attitude angles are presented in Figure 7 for the entire duration of the Jason-3 operational phase (February 2016–April 2022) before transitioning to an interleaved orbit (after the end of Sentinel-6A MF tandem phase). The temporal resolution of all time series in Figure 7 is 9.915 days, which corresponds to the repeat period of Jason-3. Each sample represents a different cycle, with the entire time series spanning 226 cycles. The presence of an attitude angle for a specific cycle does not necessarily denote an operation of the corresponding transponder. For example, the calculation of attitude angles for the GVD1 transponder location is performed for the entire duration of Jason-3 altimetric phase, although operation of the GVD1 transponder commenced in October 2021. Therefore, all attitude angles for the GVD1 D018 and GVD1 A109 times series before October 2021 are referred to the Jason-3 TCA over the "apparent" GVD1 transponder location. Obtaining a complete time series for the GVD1 site increases the confidence of spectral analysis on attitude angles.

Due to the relatively short time period (11 s; see Figure 3) it takes Jason-3 to travel from the CDN1 Cal/Val site in Crete to the GVD1 Cal/Val site in Gavdos, the attitude angles remain almost unchanged, and thus the CDN1 D018 and GVD1 D018 time series overlap (Figure 7). From the results of Figure 7, an incident of abnormal roll ($\theta_r = 7.25^\circ$) and pitch ($\theta_p = 19.58^\circ$) angles is evident in both CDN1 D018 and GVD1 D018 time series at 2020.67 (9 September 2020 22:32:43, cycle 169). These extreme angles are caused by the on-board gyro calibration, which occurred on 9 September 2020 from 22:13:36 to 23:04:55 [46]. It is worth noting that for this date, the returned waveform did not correspond to a typical point target response. Consequently, the calibration of Jason-3 could not be performed. Prior to the examination of the satellite attitude, this strange behavior of the returned waveform

could not be explained; therefore, the reason for this unsuccessful calibration was not clear to the PFAC Cal/Val team. This highlights the importance of always examining the satellite attitude and not taking for granted nominal attitude in the context of Cal/Val activities.

There are sporadic gaps in the time series of Jason-3 attitude angles in Figure 7, e.g., on26 February 2019 (cycle 112), 8 February 2020 (cycle 147) and 16 June 2020 (cycle 160), because the satellite was set on safe hold mode [46]; thus, quaternions are not available. The general behavior of the roll angle $\theta_r$ is approximately the same for all time series, with values fluctuating from $\theta_r = -0.12^\circ$ to $-0.03^\circ$. The pitch angle $\theta_p$ is positive for the descending pass D018 from $\theta_p = +0.08^\circ$ to $+0.17^\circ$ and negative for the ascending pass A109 from $\theta_p = -0.17^\circ$ to $-0.08^\circ$; hence, the pitch angle is also in agreement in terms of absolute magnitude for all time series. Finally, the yaw angle $\theta_y$ is between $-180^\circ$ and $180^\circ$ in all cases, as expected. It is worth noting that the satellite spacecraft performs recurrent yaw flip maneuvers (i.e., yaw transitions from $\theta_y = 0^\circ$ to $\pm 180^\circ$ and conversely) approximately every 58 days. These maneuvers are carried out for sufficient power inflow, and their scheduling is based on a Sun-pointing algorithm.

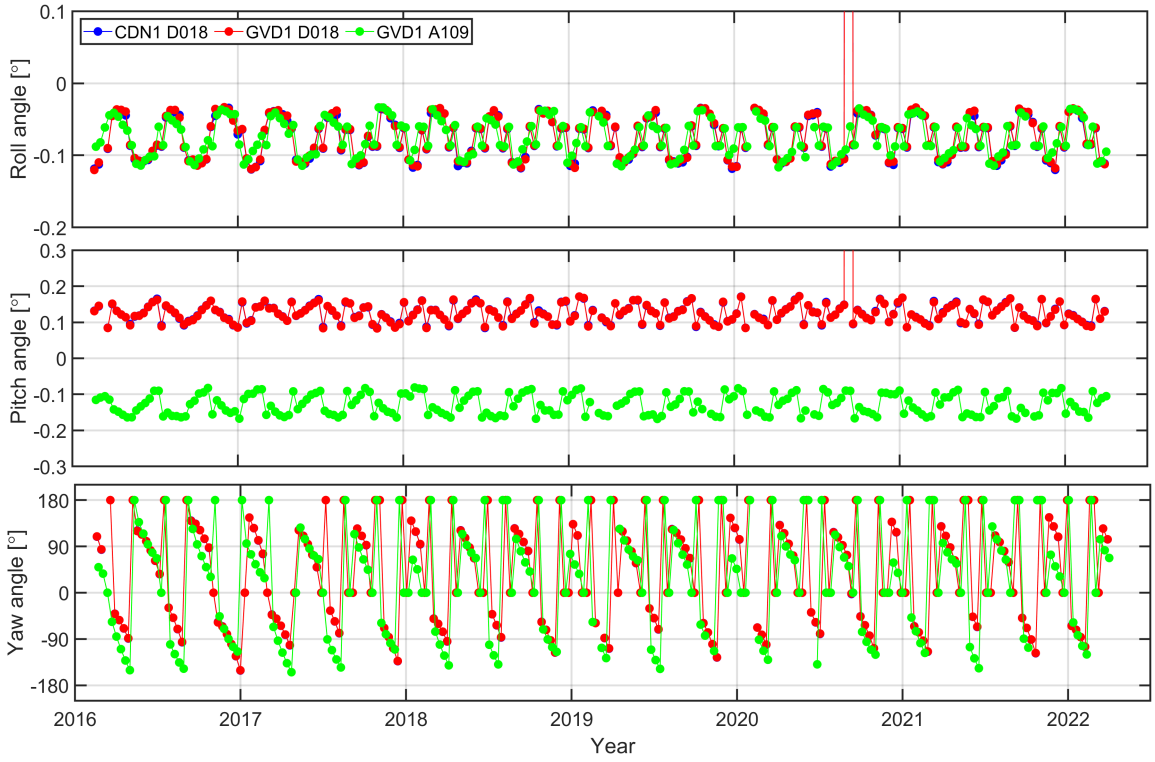


**Figure 7.** Jason-3 roll, pitch and yaw angles at CDN1 and GVD1 calibration sites.

A spectral analysis of Jason-3 attitude angles over CDN1 and GVD1 transponders was performed to identify main periodic constituents. The amplitude spectra were calculated using the standard Fast Fourier transform algorithm and are provided in Figure 8. The results reveal various periodic constituents for Jason-3 roll, pitch and yaw angles. The periodicities of the most distinct spectral peaks are estimated after applying a Hann window to the time series of Figure 7 to reduce side lobe artifacts and are summarized in Table 2. Differences were observed in both peak amplitudes and peak periodicities among the different attitude angles and satellite passes. For example, the amplitude of the roll angle at 117 days period is larger for D018 compared to A109, whereas the opposite is true for the yaw angle amplitude at 58 days period. Additionally, there were periodic constituents present in D018 amplitude spectra but not in A109, and vice versa. For example, the periodic constituent of 88 days for the yaw angle spectrum is evident in D018 but does not exist in A109. Another case is the periodic constituent of 51 days for the pitch angle, which is only present in A109 (Table 2).

For the majority of cases, the constituent with the strongest amplitude corresponds to the 117 days period, followed by the 39 days period for the roll and pitch angles and by the 58 days period for the yaw angle. Two notable exceptions are the pitch amplitude spectra for the CDN1 and GVD1 D018 passes, where the strongest amplitude is at the 39 days period with a marginally higher value than the 117 days period. Some differences in the amplitudes of the most prominent periodic constituents are also evident. For example, the D018 passes have a larger amplitude than A109 at the period of 117 days for the roll angle. The most pronounced periodic constituents (117, 58 and 39 days) of Jason-3 attitude angles are also evident in the time series of range bias, as derived from the CDN1 transponder [47]. The period of 117 days corresponds to Jason-3 draconic period (i.e., period of solar beta angle). Finally, the period of 58 days is the yaw flip-maneuver period of Jason-3 and exists only in the yaw angle spectrum, as expected.

**Table 2.** Main periods (in days) of Jason-3 attitude angles obtained by spectral analysis with a Hann window.

| | Roll | Pitch | Yaw |
|---|---|---|---|
| CDN1/GVD1 D018 | 117, 39, 32, 27, 23.5, 21 | 117, 39, 32, 27, 23.5, 21 | 117, 88, 58, 47, 39, 32, 27, 23.5, 21 |
| GVD1 A109 | 117, 39, 32, 27, 23.5, 21 | 117, 70, 51, 39, 32, 27, 23.5, 21 | 117, 58, 39, 32, 27, 23.5, 21 |

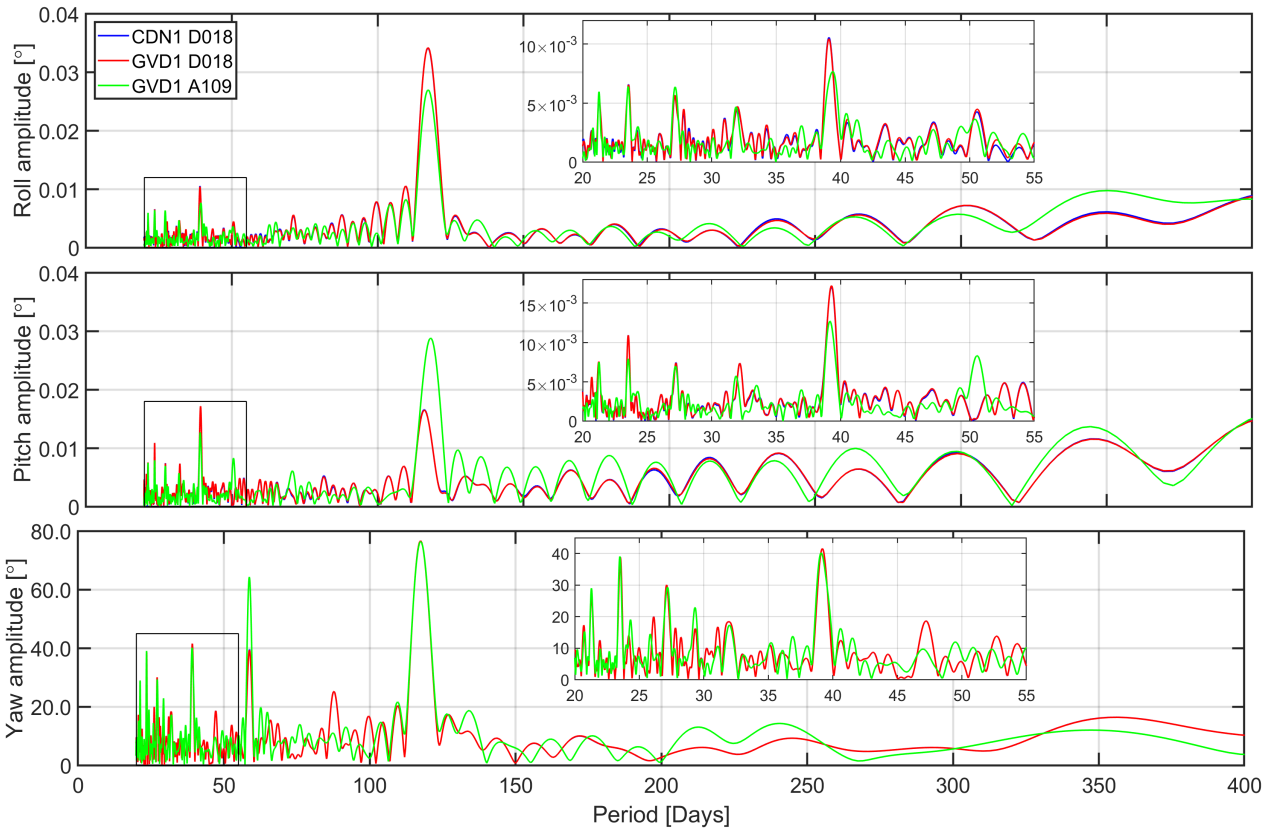


**Figure 8.** Jason-3 roll, pitch and yaw amplitude spectrum at CDN1 and GVD1 calibration sites. The framed area on the bottom left is zoomed and presented on the upper right part of the figures.

### *4.2. Jason-3 Attitude Effects on Transponder Results*

The attitude effects of the Jason-3 spacecraft on range and datation biases were derived using the methodology of Section 3.3. The time series of $\delta B$ and $\delta T$ effects for each D018 and A109 cycle with a successful calibration from CDN1 and GVD1 sites are presented in Figure 9. It is evident from the results that the attitude effect on range bias spans from

approximately −2 mm to +1 mm, whereas the effect on datation varies between ±110 μs. The two effects show an inversely proportional behavior, i.e., as $\delta B$ increases, $\delta T$ decreases. It is also apparent from Figure 9 that there are upper and lower limits for the attitude effects on $\delta T$ generated by attitude variations. The outer limits of attitude effects stem from the CoG–APC baseline length, which is constant (assuming temporal variations are negligible) and restricted by the physical dimensions of the satellite.

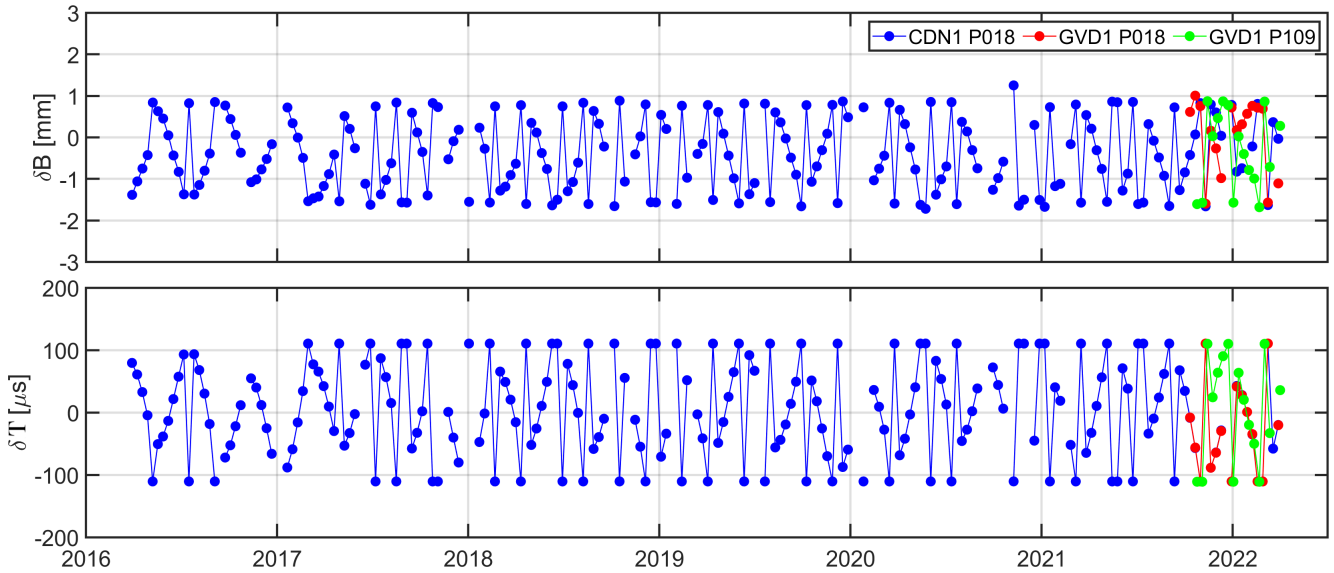


**Figure 9.** Time series of Jason-3 attitude effects on range (**top**) and datation (**bottom**) biases.

In order to identify additional patterns in the behavior of $\delta B$ and $\delta T$, we provide scatter plots of the generated attitude effects as a function of roll, pitch and yaw angles (Figure 10). From the right diagrams of Figure 10, it is evident that attitude effects become large when the yaw angle is either $\theta_y = 0°$ or $\theta_y = \pm 180°$. The APC precedes the CoG with respect to the transponder location on the ground (Table 1) when the satellite flies with $\theta_y = 0°$. In this case, the effect on range bias becomes minimum ($\delta B = -1.7$ mm), and datation grows to a maximum value ($\delta T = 110$ μs). The opposite behavior arises when the satellite flies with $\theta_y = 180°$ with CoG preceding the APC (Table 1). In this flying orientation, the effect on range bias becomes the maximum ($\delta B = 0.7$ mm), and datation comes to a minimum ($\delta T = -110$ μs). When the satellite is aligned at a right angle with respect to flight direction, where the yaw angle is $\theta_y = \pm 90°$, the impact on datation is negligible, i.e., $\delta T = 0$.

Datation seems to be affected primarily from the yaw angle. The effect of yaw attitude on $\delta T$ can be approximated using the relation:

$$\delta T \simeq \frac{\mathbf{V}_{\mathrm{SAT}}^{x} \cos\theta_y}{|\mathbf{u}|} = \frac{|\mathrm{CoG;B_0}| \cos\theta_y}{|\mathbf{u}|}, \tag{20}$$

where the $\mathbf{V}_{\mathrm{SAT}}^{x}$ is the projection component of the CoG–APC baseline vector on the $x_B$-axis in the SAT system which starts from the CoG and terminates at $\mathrm{B_0}$ as presented in Figure 5a. The $|\mathbf{u}|$ represents the magnitude of the satellite's velocity in the EFRS. In practice, Equation (20) describes the time it takes for Jason-3 to cover the distance between APC and CoG projected onto the flight direction. The values of $\delta T$ are evaluated for the complete range of yaw angles using Equation (20). The results are shown in Figure 10. It is evident that the modeled yaw effect of Equation (20) (shown with red dots on Figure 10) is in good agreement with the actual result of the analytical solution (blue dots) for datation. The attitude angles of pitch and roll seem not to significantly influence the datation as shown in Figure 10.

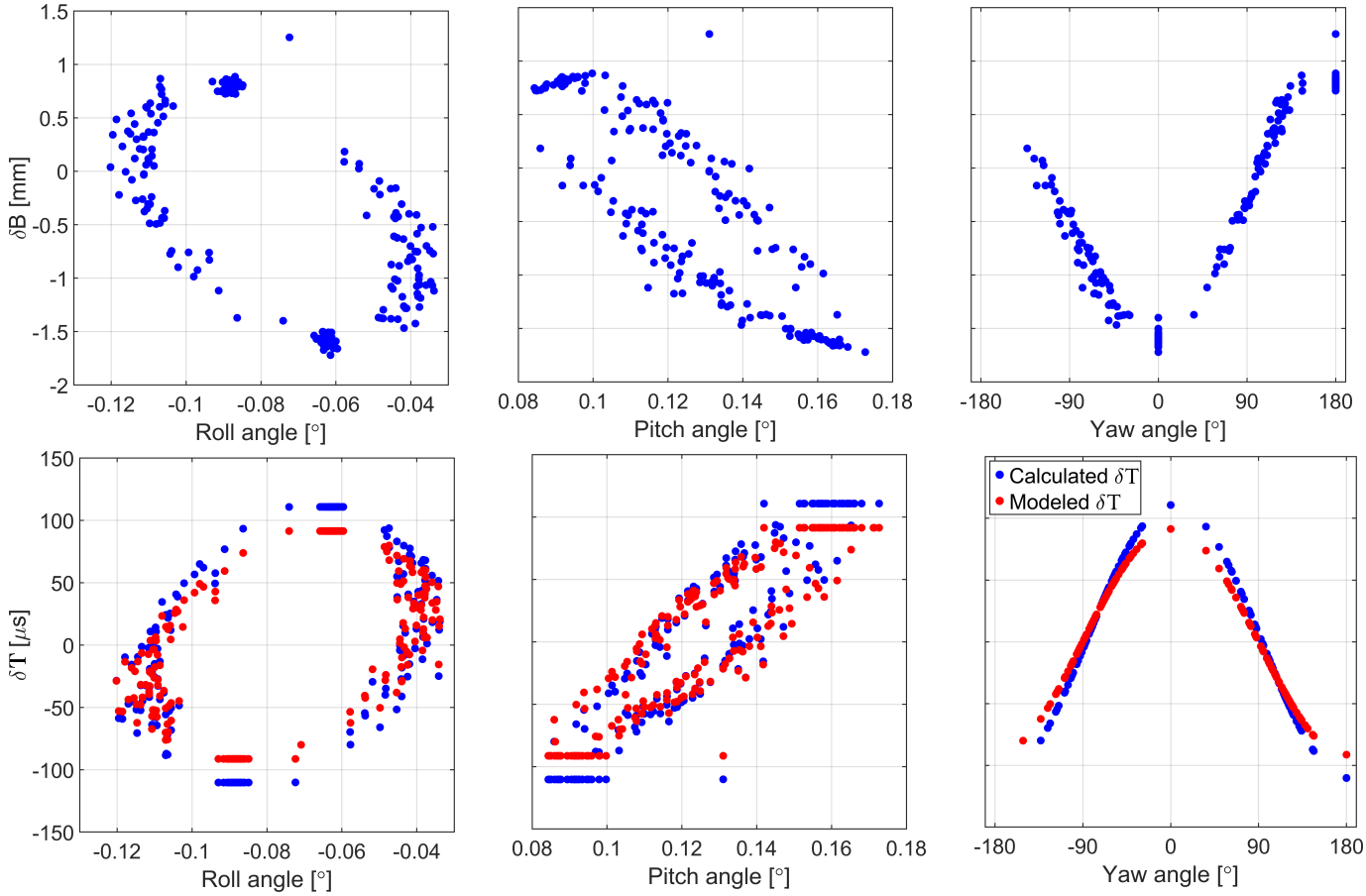


**Figure 10.** Jason-3 attitude effects $\delta B$ (**top**) and $\delta T$ (**bottom**) as a function of yaw plotted with respect to roll, pitch and yaw for the CDN1 transponder Cal/Val site and the descending pass D018.

Another spectral analysis on $\delta B$ and $\delta T$ is also performed to examine any potential propagation of periodic effects of attitude angles to biases. The spectral analysis is shown in Figure 11, and it can be seen that the periods with the greatest amplitude (in descending order of magnitude) are: 39, 23 and 117 days. These periods have already been revealed by the spectral analysis of the angles shown in Figure 8. This resemblance in periodicities corroborates the existence of effects on biases coming from attitude variations.

### *4.3. Jason-3 and Sentinel-6A MF Crossover Analysis*

The GVD1 Cal/Val site is located at a crossover point, which is defined by A109 and D018 passes of Jason-3 nominal orbit (Figure 1). The time difference between two consecutive satellite passes over GVD1 is about five days. Altimeter calibrations conducted using the GVD1 transponder offer the possibility of a crossover analysis. In this section, we calculate the range bias of Jason-3 for both A109 and D018 passes using the conventional and new calibration procedure. We then evaluate the range bias difference per cycle between A109 and D018 for each calibration procedure. This difference defines the crossover bias. It can be used to assess the altimeter performance and help identify systematic effects. The evaluation and comparison of crossover bias for the two calibration procedures can also yield valuable information regarding attitude effects on transponder results. This experiment is especially interesting for the case of Jason-3 since the spacecraft passes over GVD1 with opposite pitch angles (positive pitch angle for D18 and negative pitch angle for A109), as presented in Figure 7. The same crossover analysis is also performed for Sentinel-6A MF mission, as its orbital characteristics are identical to Jason-3.

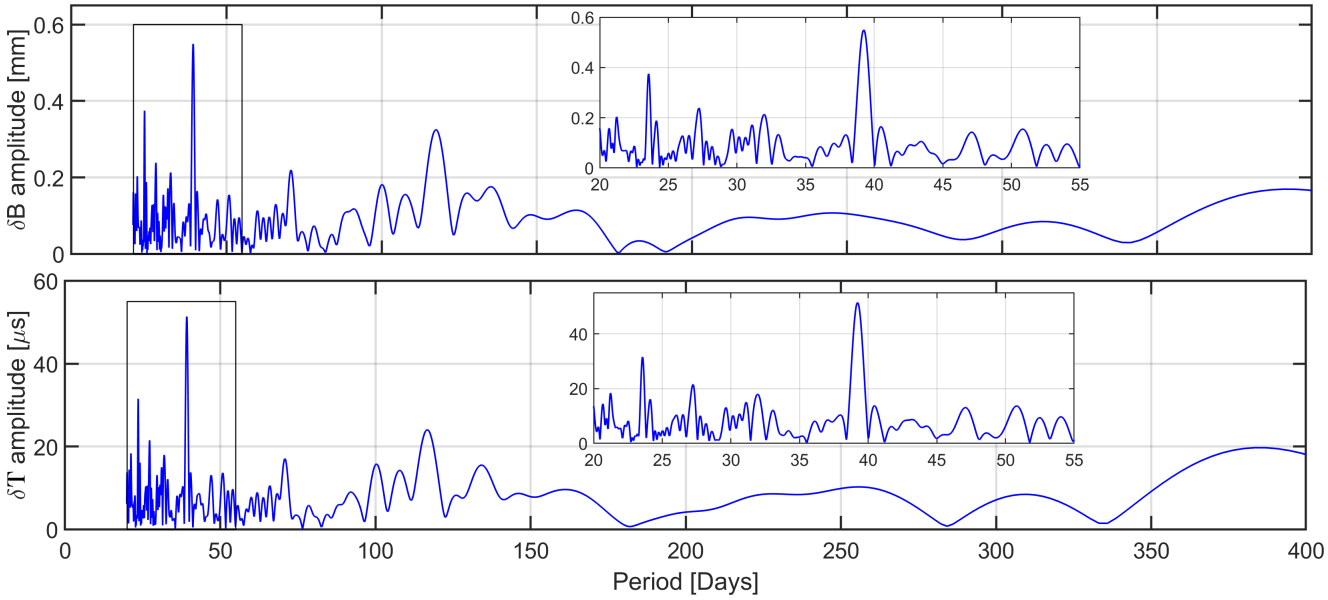


**Figure 11.** Amplitude spectrum of Jason-3 attitude effects on range and datation bias on CDN1 D018. The framed area on the bottom left is zoomed and presented on the upper right part of the figures.

According to the results, the proposed calibration procedure improves the Jason-3 crossover bias. Specifically, the mean difference between D018 and A109 using the new calibration is reduced to 7 mm and shows an improvement of 12% compared to conventional calibration (Figure 12). The absence of results for cycles 216 and 225 is because the GVD1 transponder was not operational during that time. The level of improvement presented here is comparable with the results of Jason-3 sea surface height (SSH) crossover analysis reported in Bloßfeld et al. [18]. In their study, the calculation of SSH is based on orbits estimated using model-based and observation-based attitude realization.

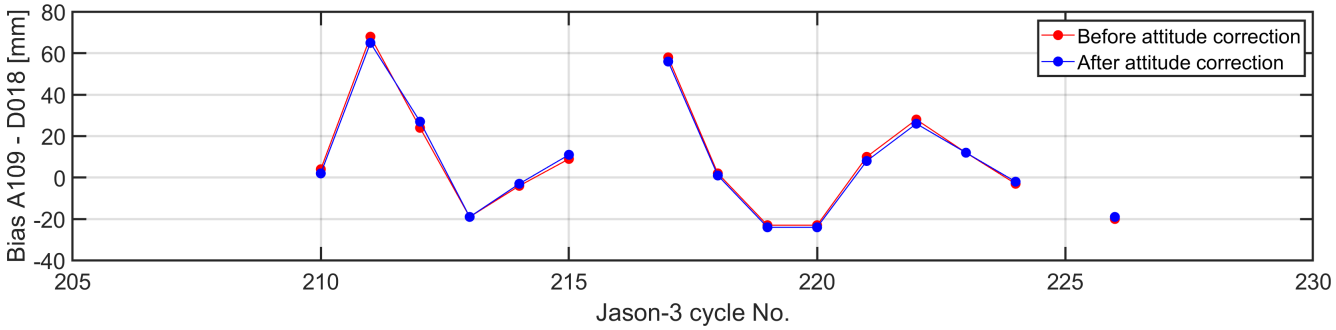


**Figure 12.** Jason-3 crossover bias determined by the GVD1 transponder using the conventional (red) and new (blue) calibration procedure.

The results of Sentinel-6A MF crossover analysis are presented in Figure 13. Implementing the proposed calibration procedure on Sentinel-6A MF also results in better agreement between the range bias of the ascending and descending pass. In this case, the averaged crossover bias is reduced from 28 mm to 24 mm, which corresponds to an improvement of 14%. It should be emphasized that the results with the new calibration procedure are preliminary, as the quaternions used (obtained by the Eumetsat Observation Portal) may not provide accurate satellite orientation. According to the documentation [48], these quaternions indeed contain information regarding the satellite orientation but were produced primarily for radio occultation analysis. The use of this dataset is motivated by the fact that it was the only readily available attitude information for Sentinel-6A MF during the time that the present analysis was conducted. Therefore, the Sentinel-6A crossover

analysis results may change when attitude quaternions for altimetry processing become publicly available [48].

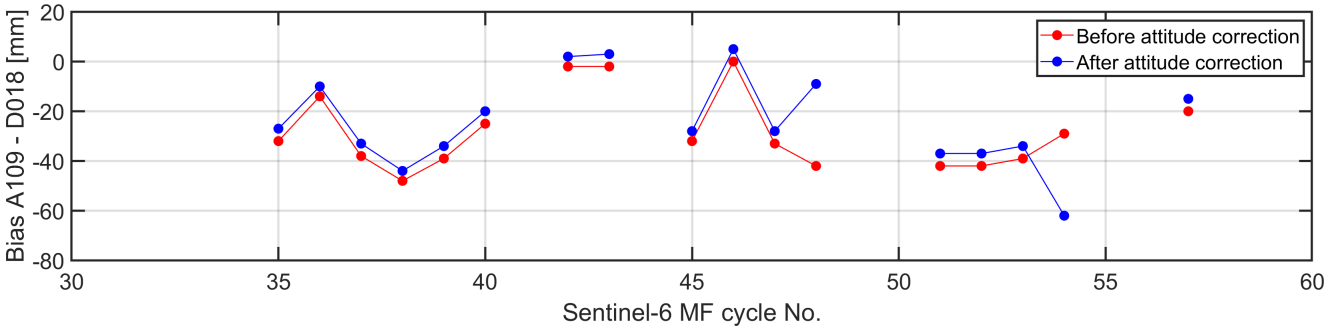


**Figure 13.** Sentinel-6A MF crossover bias determined by the GVD1 transponder using the conventional (red) and new (blue) calibration procedure.

## 5. Conclusions

In this work, we have demonstrated that the measured range used in altimeter calibration with a transponder is not correctly referred to the satellite CoG because of attitude changes. We propose an improved calibration procedure, where measured and geometric ranges are referred to the same and specific reference point. In our case, this reference point is chosen to be the APC. The estimation of the new geometric range between the transponder and the APC requires the APC coordinates in the EFRS. These are determined using the three-dimensional baseline vector between CoG and APC and satellite attitude.

The evaluation of the differences between the conventional and improved calibration procedure allows the examination of attitude effects on range and datation biases. We study these effects for Jason-3, which was the reference mission for approximately six years (2016–2022). At first the Jason-3 attitude angles (i.e., roll, pitch and yaw) are determined over the CDN1 and GVD1 transponder sites. A spectral analysis revealed periodic constituents with periods of 117, 39 and 23 days in all attitude angles. The same periodic constituents are also evident in the time series of range bias of the CDN1 transponder. This can serve as a first evidence indicating that satellite attitude affects the transponder Cal/Val results.

Jason-3 attitude effects on range and datation biases show a fluctuation from $-2$ mm to +1 mm and $\pm 110$ µs, respectively. The magnitude of attitude effects on datation bias corresponds to about 30% of its total value per cycle. These results indicate that non-ideal attitude has a strong impact on datation bias. The minimum and maximum values of attitude effects on datation bias emerge for a yaw angle of $\theta_y = 180^\circ$ ($-110$ µs) and $\theta_y = 0^\circ$ (+110 µs), respectively. This is due to the relative position and orientation of APC and CoG points in space as they pass over the transponder (i.e., which point precedes with respect to an observer at the transponder). The attitude effect is minimized when the satellite is flying with a yaw angle $\theta_y = 90^\circ$ because both APC and CoG points pass over the transponder at the same time. The attitude effects on datation bias can be predicted to a large extent using an analytical expression that is a function of the yaw angle and the x-axis distance between APC and CoG in the SAT system.

An additional analysis was conducted at the Jason-3/Setinel-6 MF crossover point over the GVD1 transponder to assess the proposed calibration procedure. The agreement of range bias between the ascending (A109) and descending (D018) pass using the new calibration procedure showed an improvement of 12% for Jason-3 and 14% for Sentinel-6A MF compared to the conventional procedure. We note that the Sentinel-6A MF results are preliminary and may change when updated quaternions become available. The level of improvement for Jason-3 is comparable with previous studies Bloßfeld et al. [18], Li et al. [19], where similar crossover analyses were performed in the context of SLR orbit determination and POD to assess the use of observation-based attitude realization.

The proposed calibration procedure is comprehensive and can be applied to every past, current and future mission with available attitude measurements. Thus, it offers

the capability for a more accurate and objective comparison of transponder calibration results from different altimetry missions by removing the influence of systematic effects that depend on both physical characteristics (e.g., internal geometric structure) and attitude realization of each satellite. The new calibration procedure is not computationally demanding and can be easily implemented by any Cal/Val team. Most importantly, it solely depends on publicly available data (i.e., attitude quaternions and GDR products) that do not require any type of pre-processing from the distribution agencies.

A reanalysis of transponder results using the proposed procedure can be performed for present and past altimetry missions, resulting in an updated estimation of range and datation biases, including relative biases between missions. The evaluation of attitude effects on calibration with a transponder can also be tested on satellite altimetry missions equipped with an interferometric radar altimeter, such as the operating CryoSat-2 [49], and the upcoming missions of Surface Water and Ocean Topography (SWOT) [50], the Copernicus polaR Ice and Snow Topography ALtimeter (CRISTAL) [51] and Guanlan [52]. For these missions, the accurate knowledge of the interferometric baseline orientation and length in three-dimensional space is an absolute prerequisite for their nominal operation. Apart from attitude effects, a possible impact of the phase center variation of the altimeter antenna on transponder results can also be evaluated. Modelling and accounting for all these effects can lead to even more rigorous calibration procedures.

**Author Contributions:** Conceptualization, C.K. and D.P.; methodology, C.K.; software, D.P.; validation, C.K., D.P., S.P.M.; formal analysis, C.K., D.P., S.P.M.; investigation, C.K. and D.P.; resources, S.P.M.; data curation, C.K., D.P., S.P.M.; writing—original draft preparation, C.K. and D.P.; writing—review and editing, S.P.M.; visualization, C.K., D.P., S.P.M.; supervision, S.P.M.; project administration, S.P.M.; funding acquisition, S.P.M. All authors have read and agreed to the published version of the manuscript.

**Funding:** This work has been produced with the financial assistance of the European Union and the European Space Agency under the project FRM4S6 (Fiducial Reference Systems for Sentinel-6A MF, No. 4000129892/20/NL/FF/ab). The views expressed herein can in no way be taken to reflect the official opinion of the European Union and/or European Space Agency.

**Data Availability Statement:** Jason-3 body quaternion files are available through NASA's Crustal Dynamics Data Information System (CDDIS) server at ftp://cddis.gsfc.nasa.gov/doris/ancillary/quaternions/, accessed on 1 September 2022. The Jason-3 mass and CoG history file is available through International DORIS Service (IDS) server at ftp://ftp.ids-doris.org/pub/ids/satellites/ja3mass.txt, accessed on 1 September 2022 and the history of satellite maneuvers at ftp://ftp.ids-doris.org/pub/ids/satellites/ja3att.txt, accessed on 1 September 2022. The quaternion files for Sentinel-6A MF analysis was downloaded from Eumetsat Observation Portal at https://eoportal.eumetsat.int, accessed on 1 September 2022.

**Acknowledgments:** The help and support of Achilles Tripolitsiotis from Space Geomatica and Xenofon Frantzis from the Technical University of Crete was invaluable and improved this work immensely. In addition, we thank very much Milen Tahtadjiev and the altimetry team at Eumetsat for making available to us the Sentinel-6A MF quaternions.

**Conflicts of Interest:** The authors declare no conflict of interest.

## Abbreviations

The following abbreviations are used in this manuscript:

| | |
|---|---|
| ADCS | Attitude Determination and Control System |
| APC | Altimeter Phase Center |
| Cal/Val | Calibration and Validation |
| CDDIS | Crustal Dynamics Data Information System |
| CoG | Center of Gravity |
| CRS | Celestial Reference System |
| DORIS | Doppler Orbitography and Radiopositioning Integrated by Satellite |
| ECV | Essential Climate Variables |

| | |
|---|---|
| EFRS | Earth-fixed reference system |
| ESA | European Space Agency |
| GCRS | Geocentric Celestial Reference System |
| GNSS | Global Navigation Satellite System |
| ICRS | International Celestial Reference System |
| IDS | International DORIS Service |
| ORB | Orbital Reference Frame |
| PCA | Point of Closest Approach |
| PFAC | Permanent Facility for Altimeter Calibration |
| POD | Precise Orbit Determination |
| PTR | Point Target Response |
| RPY | Local Orbital Reference or Roll-Pitch-Yaw system |
| SAR | Synthetic Aperture Radar |
| SAT | Satellite body reference frame |
| Sentinel-6A MF | Sentinel-6A Michael Freilich |
| SIRAL | SAR/Interferometric Radar Altimeter |
| SLR | Satellite Laser Ranging |
| TCA | Time of Closest Approach |
| TOPEX | Ocean Topography Experiment |
| TRP | Transponder |
| USO | Ultra-Stable Oscillator |

## References


1. Gornitz, V. Monitoring sea level changes. *Clim. Chang.* **1995**, *31*, 515–544. [CrossRef]
2. Haigh, I.D.; Wahl, T.; Rohling, E.J.; Price, R.M.; Pattiaratchi, C.B.; Calafat, F.M.; Dangendorf, S. Timescales for detecting a significant acceleration in sea level rise. *Nat. Commun.* **2014**, *5*, 3635. [CrossRef] [PubMed]
3. Carlowicz, M. Sea Level Rise Hits Home at NASA: Watching Water Rise Right Outside the Front Door. 2015. Available online: https://earthobservatory.nasa.gov/features/NASASeaLevel (accessed on 26 August 2015).
4. Bojinski, S.; Verstraete, M.; Peterson, T.C.; Richter, C.; Simmons, A.; Zemp, M. The concept of essential climate variables in support of climate research, applications, and policy. *Bull. Am. Meteorol. Soc.* **2014**, *95*, 1431–1443. [CrossRef]
5. Hollmann, R.; Merchant, C.J.; Saunders, R.; Downy, C.; Buchwitz, M.; Cazenave, A.; Chuvieco, E.; Defourny, P.; de Leeuw, G.; Forsberg, R.; et al. The ESA climate change initiative: Satellite data records for essential climate variables. *Bull. Am. Meteorol. Soc.* **2013**, *94*, 1541–1552. [CrossRef]
6. Fu, L.L.; Le Traon, P.Y. Satellite altimetry and ocean dynamics. *Comptes Rendus Geosci.* **2006**, *338*, 1063–1076. [CrossRef]
7. Vignudelli, S.; Birol, F.; Benveniste, J.; Fu, L.L.; Picot, N.; Raynal, M.; Roinard, H. Satellite altimetry measurements of sea level in the coastal zone. *Surv. Geophys.* **2019**, *40*, 1319–1349. [CrossRef]
8. Calmant, S.; Crétaux, J.F.; Rémy, F. Principles of radar satellite altimetry for application on inland waters. In *Microwave Remote Sensing of Land Surface*; Elsevier: Amsterdam, The Netherlands, 2016; pp. 175–218.
9. Foresta, L.; Gourmelen, N.; Pálsson, F.; Nienow, P.; Björnsson, H.; Shepherd, A. Surface elevation change and mass balance of Icelandic ice caps derived from swath mode CryoSat-2 altimetry. *Geophys. Res. Lett.* **2016**, *43*, 12–138. [CrossRef]
10. Archer, M.R.; Li, Z.; Fu, L.L. Increasing the space–time resolution of mapped sea surface height from altimetry. *J. Geophys. Res. Ocean.* **2020**, *125*, e2019JC015878. [CrossRef]
11. Timmermans, B.; Gommenginger, C.; Dodet, G.; Bidlot, J.R. Global wave height trends and variability from new multimission satellite altimeter products, reanalyses, and wave buoys. *Geophys. Res. Lett.* **2020**, *47*, e2019GL086880. [CrossRef]
12. Abdalla, S. Ku-band radar altimeter surface wind speed algorithm. *Mar. Geod.* **2012**, *35*, 276–298. [CrossRef]
13. Ray, R.D. Daily harmonics of ionospheric total electron content from satellite altimetry. *J. Atmos. Sol.-Terr. Phys.* **2020**, *209*, 105423. [CrossRef]
14. Rose, S.K.; Andersen, O.B.; Passaro, M.; Ludwigsen, C.A.; Schwatke, C. Arctic Ocean sea level record from the complete radar altimetry era: 1991–2018. *Remote Sens.* **2019**, *11*, 1672. [CrossRef]
15. Müller, F.L.; Wekerle, C.; Dettmering, D.; Passaro, M.; Bosch, W.; Seitz, F. Dynamic ocean topography of the northern Nordic seas: A comparison between satellite altimetry and ocean modeling. *Cryosphere* **2019**, *13*, 611–626. [CrossRef]
16. Powell, R.J. Relative Vertical Positioning Using Ground-Level Transponders with the ERS-1 Altimeter. *IEEE Trans. Geosci. Remote. Sens.* **1986**, *GE-24*, 421–425. [CrossRef]
17. Willis, J.; Bonnefond, P.; Leuliette, E.; Scharroo, R.; Donlon, C. *Report of the Ocean Surface Topography Science Team Meeting*; OSTST Technical Report; NASA: Washington, DC, USA; CNES: Pairs, France; NOAA: Washington, DC, USA; EUMETSAT: Darmstadt, Germany; ESA: Pairs, France; Ocean Surface Topography Science Team Symposium Summary: Chicago, IL, USA, 2019.
18. Bloßfeld, M.; Zeitlhöfler, J.; Rudenko, S.; Dettmering, D. Observation-based attitude realization for accurate jason satellite orbits and its impact on geodetic and altimetry results. *Remote Sens.* **2020**, *12*, 682. [CrossRef]
19. Li, K.; Zhou, X.; Guo, N.; Zhou, S. Effect of PCV and attitude on the precise orbit determination of Jason-3 satellite. *J. Appl. Geod.* **2022**, *16*, 143–150. .:10.1515/jag-2021-0052. [CrossRef]
20. Hayne, G.; Hancock, D., III. Corrections for the effects of significant wave height and attitude on Geosat radar altimeter measurements. *J. Geophys. Res. Ocean.* **1990**, *95*, 2837–2842. [CrossRef]

21. Hayne, G.; Hancock, D., III.; Purdy, C.; Callahan, P. The corrections for significant wave height and attitude effects in the TOPEX radar altimeter. *J. Geophys. Res. Ocean.* **1994**, *99*, 24941–24955. [CrossRef]
22. Amarouche, L.; Thibaut, P.; Zanife, O.Z.; Dumont, J.P.; Vincent, P.; Steunou, N. Improving the Jason-1 ground retracking to better account for attitude effects. *Mar. Geod.* **2004**, *27*, 171–197. [CrossRef]
23. Sepulveda, H.H.; Queffeulou, P.; Ardhuin, F. Assessment of SARAL/AltiKa wave height measurements relative to buoy, Jason-2, and Cryosat-2 data. *Mar. Geod.* **2015**, *38*, 449–465. [CrossRef]
24. Galin, N.; Wingham, D.J.; Cullen, R.; Francis, R.; Lawrence, I. Measuring the pitch of CryoSat-2 using the SAR mode of the SIRAL altimeter. *IEEE Geosci. Remote Sens. Lett.* **2014**, *11*, 1399–1403. [CrossRef]
25. Watson, C.; White, N.; Church, J.; Burgette, R.; Tregoning, P.; Coleman, R. Absolute calibration in bass strait, Australia: TOPEX, Jason-1 and OSTM/Jason-2. *Mar. Geod.* **2011**, *34*, 242–260. [CrossRef]
26. Cristea, E.; Moore, P. Altimeter bias determination using two years of transponder observations. *Proc. Envisat Symp.* **2007**, 23–27.
27. Hausleitner, W.; Moser, F.; Desjonqueres, J.D.; Boy, F.; Picot, N.; Weingrill, J.; Mertikas, S.; Daskalakis, A. A new method of precise Jason-2 altimeter calibration using a microwave transponder. *Mar. Geod.* **2012**, *35*, 337–362. [CrossRef]
28. Quartly, G.D.; Rinne, E.; Passaro, M.; Andersen, O.B.; Dinardo, S.; Fleury, S.; Guerreiro, K.; Guillot, A.; Hendricks, S.; Kurekin, A.A.; et al. Review of radar altimetry techniques over the Arctic ocean: Recent progress and future opportunities for sea level and sea ice research. In *The Cryosphere Discussions*; European Geosciences Union: Munich, Germany, 2018; pp. 1–51.
29. Mertikas, S.; Tripolitsiotis, A.; Donlon, C.; Mavrocordatos, C.; Féménias, P.; Borde, F.; Frantzis, X.; Kokolakis, C.; Guinle, T.; Vergos, G.; et al. The ESA Permanent Facility for altimetry calibration: Monitoring performance of radar altimeters for Sentinel-3A, Sentinel-3B and Jason-3 using transponder and sea-surface calibrations with FRM standards. *Remote Sens.* **2020**, *12*, 2642. [CrossRef]
30. Wei, G.; Xiao-Yan, G.; Xi-Yu, X.; Liu, H.G.; Chuan-Dong, X.; Yue-Heng, D. A transponder system dedicating for the on-orbit calibration of China's new-generation satellite altimeter and scatterometer. In Proceedings of the 2011 IEEE CIE International Conference on Radar, Chengdu, China, 24–27 October 2011; Volume 1, pp. 22–25.
31. Wang, C.; Lin, M.; Ma, C.; Xu, K.; Liu, P.; Wang, T.; Mu, B.; Zhu, J.; Guo, W. In-orbit calibration and validation of HY-2B altimeter using an improved transponder. *IEEE J. Sel. Top. Appl. Earth Obs. Remote Sens.* **2021**, *14*, 10162–10173. [CrossRef]
32. Birks, A. Radar altimeter calibration using ground based transponders. In Proceedings of the ERS-ENVISAT Symposium, Gothenburg, Sweden, 16–20 October 2000; pp. 23–27.
33. Mertikas, S.P.; Donlon, C.; Féménias, P.; Mavrocordatos, C.; Galanakis, D.; Tripolitsiotis, A.; Frantzis, X.; Tziavos, I.N.; Vergos, G.; Guinle, T. Fifteen years of Cal/Val service to reference altimetry missions: Calibration of satellite altimetry at the Permanent Facilities in Gavdos and Crete, Greece. *Remote Sens.* **2018**, *10*, 1557. [CrossRef]
34. Donlon, C.J.; Minnett, P.J.; Fox, N.; Wimmer, W. Strategies for the laboratory and field deployment of ship-borne fiducial reference thermal infrared radiometers in support of satellite-derived sea surface temperature climate data records. In *Experimental Methods in the Physical Sciences*; Elsevier: Amsterdam, The Netherlands, 2014; Volume 47, pp. 557–603.
35. Mertikas, S.P.; Donlon, C.; Féménias, P.; Cullen, R.; Galanakis, D.; Frantzis, X.; Tripolitsiotis, A. Fiducial Reference Measurements for Satellite Altimetry Calibration: The Constituents. In *Fiducial Reference Measurements for Altimetry*; Springer: Berlin/Heidelberg, Germany, 2019; pp. 1–6.
36. Mertikas, S.; Partsinevelos, P.; Tripolitsiotis, A.; Kokolakis, C.; Petrakis, G.; Frantzis, X. Validation of Sentinel-3 OLCI integrated water vapor products using regional GNSS measurements in crete, Greece. *Remote Sens.* **2020**, *12*, 2606. [CrossRef]
37. Cerri, A.L. Couhert, P.F. *DORIS Satellites Models Implemented in POE Processing;* Technical Report: SALP-NT-BORD-OP-16137-CN; Centre National d'ètudes Spatiales: Paris, France, 2022.
38. Perrygo, C. TOPEX satellite yaw maneuvers. *IOC* **1987**, *968*, 87–074.
39. Zeitlhöfler, J. Nominal and observation-based attitude realization for precise orbit determination of the Jason satellites. Master's Thesis, Technical University of Munich, Department of Civil, Geo and Environmental Engineering: Munich, Germany, 2019.
40. Vallado, D.A. *Fundamentals of Astrodynamics and Applications*; Springer Science & Business Media: Berlin/Heidelberg, Germany, 2001; Volume 12.
41. Brown, G. The average impulse response of a rough surface and its applications. *IEEE Trans. Antennas Propag.* **1977**, *25*, 67–74. [CrossRef]
42. Garcia-Mondéjar, A.; Fornari, M.; Bouffard, J.; Féménias, P.; Roca, M. CryoSat-2 range, datation and interferometer calibration with Svalbard transponder. *Adv. Space Res.* **2018**, *62*, 1589–1609. [CrossRef]
43. Petit, G.; Luzum, B. *IERS Technical Note No. 36, IERS Conventions (2010);* Technical Report; International Earth Rotation and Reference Systems Service: Frankfurt, Germany, 2010.
44. Luzum, B.; Petit, G. The IERS Conventions (2010): Reference systems and new models. *Proc. Int. Astron. Union* **2012**, *10*, 227–228. [CrossRef]
45. Giulicchi, L. *Sentinel-6 Michael Freilich POD Context;* Technical Report JC-TN-ESA-SY-0420; European Space Agency: Paris, France, 2022.
46. Roinard, L.M.H. *Jason-3 Validation and Cross Calibration Activities (Annual Report 2020);* Technical Report SALP-RP-MA-EA-23473-CLS; Collecte Localisation Satellites: Toulouse, France, 2021.

47. Mertikas, S.P.; Donlon, C.; Mavrocordatos, C.; Piretzidis, D.; Kokolakis, C.; Cullen, R.; Matsakis, D.; Borde, F.; Fornari, M.; Boy, F.; et al. Performance evaluation of the CDN1 altimetry Cal/Val transponder to internal and external constituents of uncertainty. *Adv. Space Res.* **2022**, *70*, 2458–2479. [CrossRef]
48. EUMETSAT. *Jason-CS/Sentinel-6 RO Level 1B Auxiliary Data Specification;* Technical Report EUM/LEO-JASCS/SPE/16/882105; EUMETSAT: Darmstadt, Germany, 2022.
49. Armitage, T.W.; Davidson, M.W. Using the interferometric capabilities of the ESA CryoSat-2 mission to improve the accuracy of sea ice freeboard retrievals. *IEEE Trans. Geosci. Remote Sens.* **2013**, *52*, 529–536. [CrossRef]
50. Morrow, R.; Fu, L.L.; Ardhuin, F.; Benkiran, M.; Chapron, B.; Cosme, E.; d'Ovidio, F.; Farrar, J.T.; Gille, S.T.; Lapeyre, G.; et al. Global observations of fine-scale ocean surface topography with the Surface Water and Ocean Topography (SWOT) mission. *Front. Mar. Sci.* **2019**, *6*, 232. [CrossRef]
51. Kern, M.; Cullen, R.; Berruti, B.; Bouffard, J.; Casal, T.; Drinkwater, M.R.; Gabriele, A.; Lecuyot, A.; Ludwig, M.; Midthassel, R.; et al. The Copernicus Polar Ice and Snow Topography Altimeter (CRISTAL) high-priority candidate mission. *Cryosphere* **2020**, *14*, 2235–2251. [CrossRef]
52. Chen, G.; Tang, J.; Zhao, C.; Wu, S.; Yu, F.; Ma, C.; Xu, Y.; Chen, W.; Zhang, Y.; Liu, J.; et al. Concept design of the "Guanlan" science mission: China's novel contribution to space oceanography. *Front. Mar. Sci.* **2019**, *6*, 194. [CrossRef]